Structural analysis of a Laramide, basement-involved, foreland fault zone, Rawlins uplift, south-central Wyoming

Aaron S. Otteman[1] and Arthur W. Snoke*

Department of Geology and Geophysics, Dept. 3006, 1000 East University Avenue, University of Wyoming, Laramie, WY 82071, U.S.A.

[1]Present address: ExxonMobil Production Company, 396 West Greens Road, CORP-WGR-207, Houston, TX 77067, U.S.A.

**Correspondence should be addressed to: snoke@uwyo.edu*

ABSTRACT

The western border of the Hanna Basin is defined by the Rawlins uplift, a Laramide, basement-involved, faulted arch. This north-northwest–south-southeast-trending structure separates the Hanna Basin on the east from the Great Divide Basin (part of the greater Green River depositional basin) on the west. The Rawlins uplift is a west–southwest-vergent, macroscale, fault-related fold. Detailed geologic mapping, construction of serial cross sections, and the incorporation of data from a seismic-reflection profile indicate that displacement along the fault zone flanking the uplift's western margin cannot account for the net structural relief between the Hanna and Great Divide Basins (~37,000 vertical ft [~11,285 vertical m] and ~27,000 vertical ft [~8,235 vertical m], respectively). The exposed frontal fault traces are interpreted as high-angle (~70º) splays off a shallowly dipping (~25º), master fault zone developed within Archean granitic rocks of the Wyoming province. A low-dipping, braided, plastic-to-brittle thrust-fault zone in the Precambrian basement is inferred to accommodate much of the fault displacement and thus account for the structural relief between the core of the uplift and the adjacent basins. Within the study area, displacement along the exposed frontal fault zone decreases from south to north. Within the map area, bedding attitudes along the southwest limb (forelimb) of the uplift range from ~30–90º with only local areas of overturned beds. However, southwest of the map area, Upper Cretaceous strata are sub-vertical to overturned. On the homoclinal backlimb, dips are ~10–15º east-northeast into the Hanna Basin. Eastward structural bends at the southern and northern margins of the uplift suggest a component of left-lateral, oblique-slip displacement along the southern margin and right-lateral, oblique-slip displacement along the northern margin. Pre-existing basement anisotropies or discontinuities are likely responsible for these important changes in structural grain.

KEY WORDS: Laramide orogeny, fault-related arch, basement-involved uplift, brittle fault zone, Rocky Mountain foreland deformation, Rawlins uplift, Wyoming.

INTRODUCTION

Although numerous kinematic models exist for Laramide, basement-involved, foreland uplifts (e.g., Stone, 1984; Erslev, 1991; Erslev and Rogers, 1993; McConnell and Wilson, 1993; Stone, 1993a; Narr and Suppe, 1994), few detailed structural analyses based on large-scale (1:12,000 or greater), surface geologic mapping of the fault zones associated with these uplifts have been published. Notable exceptions include Hoppin (1961), Schmidt and Garihan (1983), Kellogg et al. (1995), and O'Connell (1996). In contrast, there have been detailed fault-rock and kinematic studies of these brittle fault zones (e.g., Mitra, 1984; Wise and Obi, 1992; Evans, 1993; Molzer and Erslev, 1995), as well as integrative studies that relate basement-involved deformation and the development of synorogenic sedimentary deposits (e.g., DeCelles et al., 1991; Hoy and Ridgway, 1997).

A fundamental reason for the lack of detailed geologic mapping of the Laramide fault zones is that many of the large-displacement fault zones are poorly exposed (e.g., Wind River thrust) or perhaps blind at the Earth's surface (e.g., thrust-fault zone associated with the Casper arch). However, the Laramide fault zones associated with both the Wind River Range and Casper arch have been well imaged in the subsurface by seismic-reflection profiling (e.g., Smithson et al., 1979; Skeen and Ray, 1983; Ray and Berg, 1985; Sharry et al., 1986). The results provide critical information on how basement-involved, foreland faults root into the deep crust. Also, Stone (1993a) analyzed the subsurface geometry of many Laramide fault zones based on the interpretation of seismic-reflection profiles.

The upper-crustal deformation of deep-rooted Laramide, basement-involved faulting is complex and typically involves the partitioning of strain between faulting and folding as well as local reactiviation of pre-existing crustal anisotropies (e.g., Erslev, 1991; Varga, 1993; Stone, 2002; Bump, 2003). In this context, the chief purpose of the present study was to investigate a well-exposed, Laramide, basement-involved fault zone through large-scale (1:12,000) surface geologic mapping. We chose the exposed fault zone on the southwestern margin of the Rawlins uplift for detailed analysis because it is relatively well exposed and because regional geologic mapping and stratigraphic studies are available for the entire uplift (Barlow, 1953). The Rawlins uplift is a relatively simple Laramide, basement-involved uplift that forms the western flank of the Hanna Basin, and the fault zone exposed at the Earth's surface has been interpreted as the fundamental displacement zone related to the uplift (Barlow, 1953). Another reason for studying the fault zone associated with the Rawlins uplift is the availability of regional seismic-reflection profiles. These allow us to tie our new surface geologic mapping into the subsurface.

AN OVERVIEW OF THE RAWLINS UPLIFT

The Rawlins uplift is a north-northwest–south-southeast-trending, basement-involved structure with an eastward bend along its faulted southern margin and a northeast bend (i.e., Rawlins–Bell Springs fault of Dobbin et al., 1928) at its faulted northern margin (Figs. 1 and 2). Structural relief on the basement–cover contact measured from the core area of the uplift to the central part of adjacent basins is significant. Within the uplift, the basement–cover contact is exposed at ~7,200 ft (~2,196 m) above sea level and up to ~7,600 ft (~2,318 m) above sea level in the vicinity of Rawlins Peak. The "top-of-basement" structure contour map of Blackstone (1993) places the basement–cover interface at ~30,000 ft (~9150 m) below sea level east of the Rawlins uplift in the central part of the Hanna basin (Fig. 1). Similarly, to the west, in the Great Divide basin, the basement–cover contact is ~20,000 ft (~6,100 m) below sea level (Fig. 1). The structural relief of the basement–cover contact is thus at least ~37,000+ ft (~11,285+ m) and ~27,000+ ft (~8,235+ m) from the deepest parts of the Hanna and Great Divide Basins, respectively, to the crest of the Rawlins arch.

The Rawlins uplift is a macroscale, asymmetric, fault-related fold that verges southwestward (Fig. 2) and is related to major dip-slip displacement along a basement-rooted thrust fault or faults. The core of the fold is composed of Precambrian igneous and metamorphic rocks of uncertain age, but probably chiefly Archean based on regional relationships (Chamberlain et al., 2003).

The eastward bends in the strike of the fault zones bounding the uplift at its southern and northern margins (Fig. 2) are at a high angle to the overall trend of the Rawlins arch. Thus the orientations of these bounding fault zones suggest a component of left-lateral, oblique-slip displacement along the southern margin and right-lateral, oblique-slip displacement along the northern margin. Pre-existing basement weaknesses or discontinuities may be responsible for these abrupt changes in orientation of the fault trace (Chase et al., 1993; Lillegraven et al., 2004). This speculation is supported by the east–west orientation of the fault zone along the southern margin that parallels the late Mesoproterozoic(?)–Neoproterozoic Uinta trend (Bryant, 1985; Stone, 1993b). Similarly, the northeast–southwest strike of the fault zone along the northern margin is sub-parallel to the Paleoproterozoic Cheyenne belt (Duebendorfer and Houston, 1987) as well as to other important shear zones in the Wyoming province (e.g., Resor and Snoke, 2005).

The west limb (forelimb) of the Rawlins arch is moderately to steeply dipping with attitudes ranging from ~30°–90° (Fig. 3). Within the map area, only localized areas of overturned strata occur (see Fig. 3; e.g., sec. 32, T. 22 N., R. 88 W.). However, broader regions of sub-vertical to overturned Upper Cretaceous strata occur southwest of the map area (Barlow, 1953; Fig. 2).

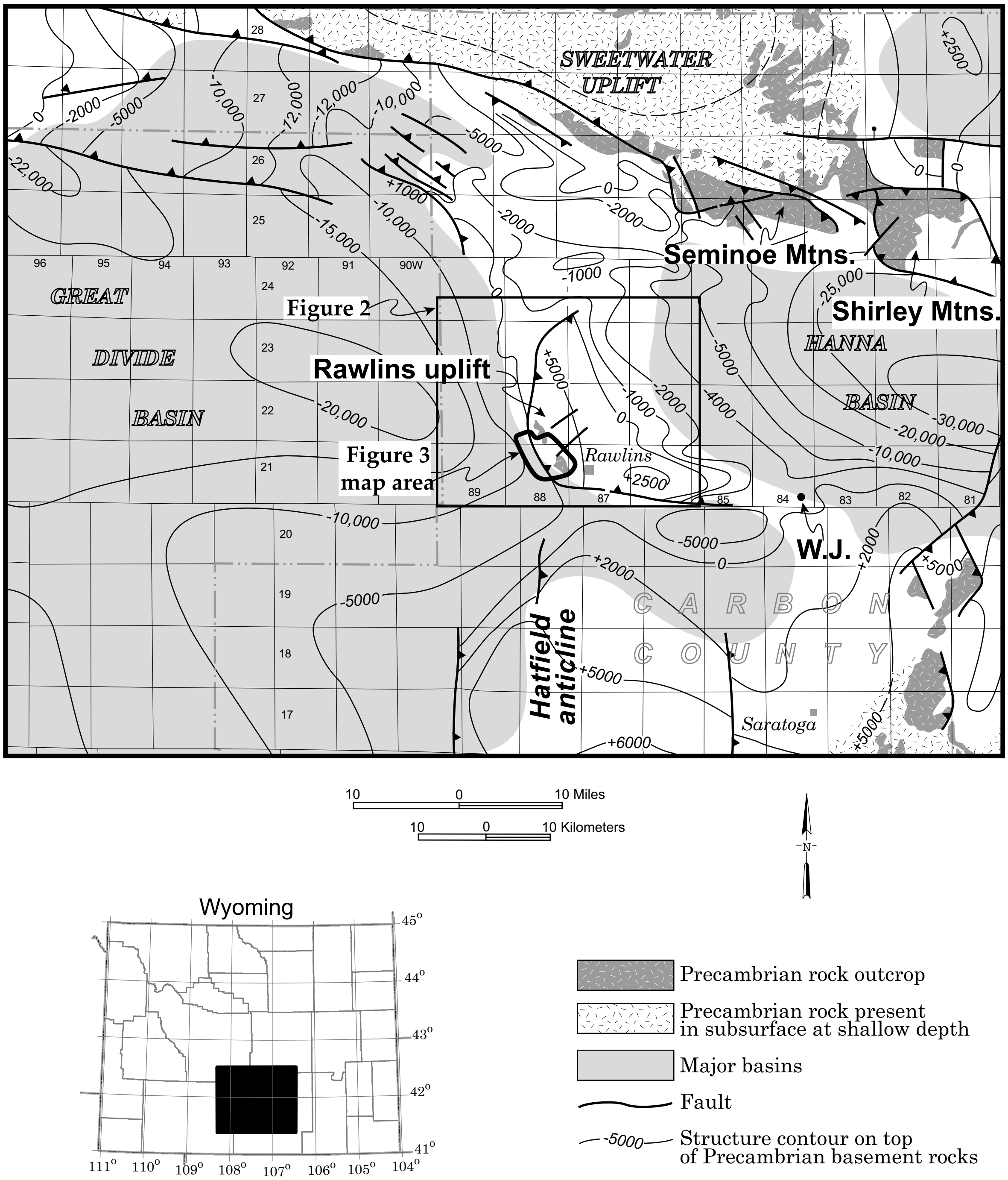

Figure 1. Regional location map derived from Blackstone's (1993) "Precambrian basement map of Wyoming: outcrop and structural configuration." Structural contours (feet below or above mean sea level) are on top of Precambrian. W.J. = Walcott Junction. Areas of Figure 2 and 3 are outlined.

Numerous "parasitic" structures are superimposed upon the large-scale fold of the uplift. The most obvious parasitic feature within the map area is the fold with a core comprised chiefly of Lower Triassic Red Peak Formation in sec. 33, T. 22 N., R. 88 W. and sec. 4, T. 21 N., R. 88 W. (Fig. 3). The hinge line of this fold plunges ~10° to the northwest, and the fold shape is asymmetric to the southwest due, in part, to bedding-plane slip and intraformational faulting within the Red Peak Formation. Within the map area, addi-

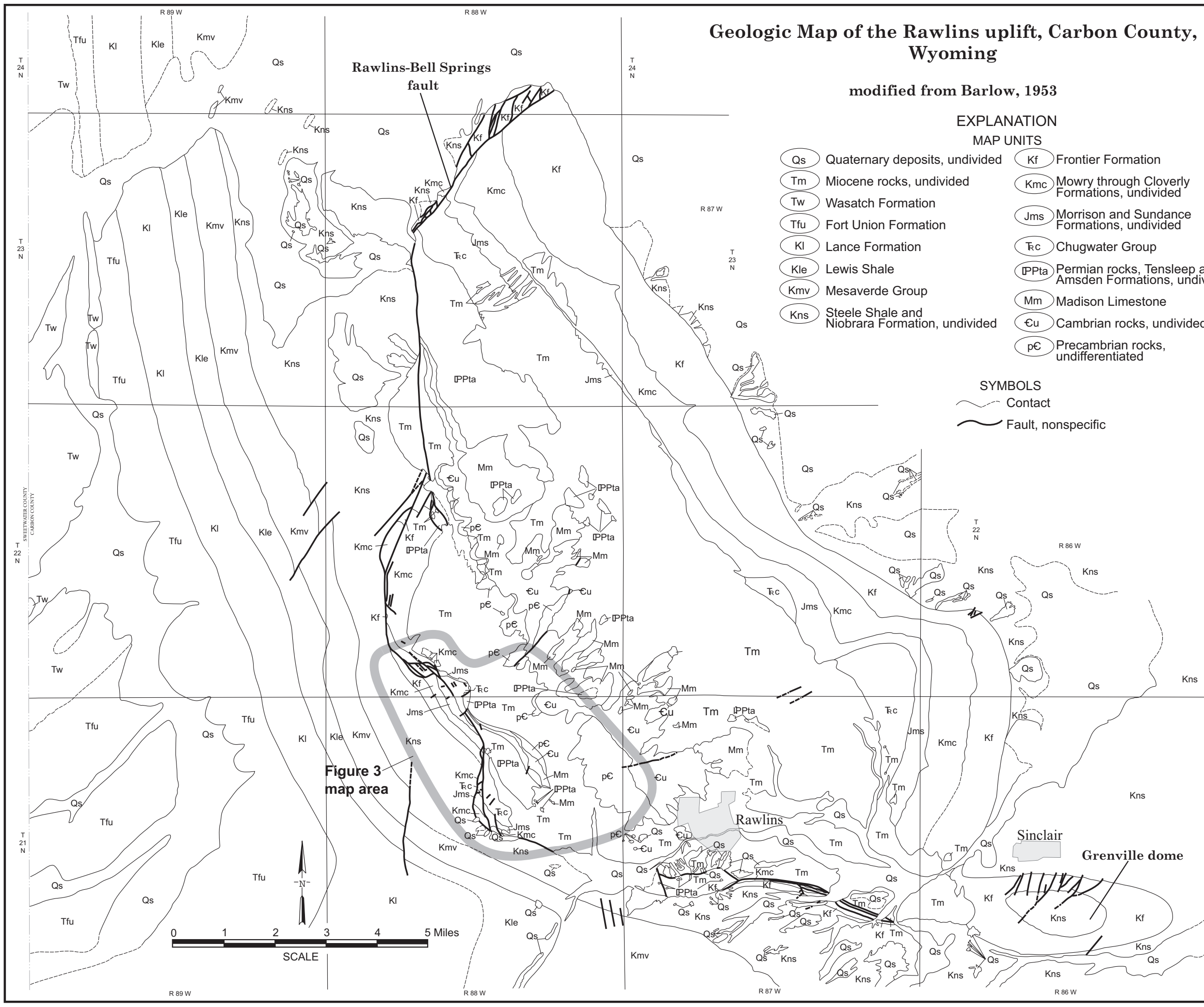

Figure 2. Generalized geologic map of Rawlins uplift (modified from Barlow, 1953) with map area (Figure 3) outlined.

tional parasitic structures are located just northwest of the aforementioned fold (Fig. 3). These structures are fault-related undulations in bedding that form a series of minor anticlines and synclines.

The exposed frontal fault zone loses overall displacement from south to north within the map area. Figure 1 shows that the minus 5,000-foot contour on the top of Precambrian basement intersects the primary frontal fault at the southwestern margin of the uplift (structural contours adapted from Blackstone, 1993). However, the 0-foot contour (sea level) intersects the primary fault to the north (Fig. 1). This inferred decrease in displacement represents a net decrease in vertical displacement (throw component of a dip-slip fault) of ~5,000 ft (~1,525 m) across about six miles (~9.7 km) of strike distance. If the fault dip were seen to progressively shallow to the north, then the inferred displacement magnitude could be maintained along strike. However, map data do not support a significant decrease in fault-plane dip along strike from south to north. The scarcity of overturned sedimentary units within the map area (Fig. 3) is consistent with a high-angle, frontal ("breaching") fault. Thus, the breaching fault associated with the Rawlins

Figure 3 (A full size, color folded map accompanies this issue, and a black-and-white thumbnail version appears on page 89). Geologic map of southwestern corner of Rawlins uplift, Carbon County, Wyoming (scale 1:12,000). Geology mapped by A. S. Otteman (2001–2003). Cross section lines A–A' through E–E' are delineated as well as the approximate location of seismic-reflection profile SPL-2.

Table 1. Stratigraphic nomenclature and thicknesses of Phanerozoic units exposed in Rawlins uplift, south-central Wyoming. Thickness data derived from field observations and Barlow (1953).

Age	Formation	Thickness	
		Meters	Feet
Quaternary	alluvial/colluvial/human disturbed deposits	0–18	0–60
---U---	gravel deposits–Quaternary–Pliocene	0–18	0–60
Tertiary	Tertiary undivided (Pliocene[?]–Miocene)	~30	~100
U			
Late Cretaceous	Niobrara and Steele Formations	1471	4825
	Frontier Formation	~256	~840
	Mowry Shale	76	250
Early Cretaceous	Muddy Sandstone	11	35
	Thermopolis Shale	11	35
	Cloverly Formation	34	110
Jurassic	Morrison Formation	85	280
	Sundance Formation	122	400
Triassic	Jelm Formation	113	370
	Alcova Limestone	5	15
	Red Peak Formation	~198	~650
Permian	Goose Egg Formation	~58	~190
Pennsylvanian	Tensleep Sandstone	274	900
	Amsden Formation	70	230
Mississippian	Madison Limestone	~53	~175
U			
Cambrian	Flathead Sandstone	91–183	300–600
U			
Precambrian	basement rocks of the Wyoming province		

uplift is inferred to be a high-angle reverse fault that dips ~70° to the east.

Furthermore, we suggest that the apparent larger displacement and obvious ramping of the frontal fault zone in the southern part of the map area is, in part, accommodated by a north-directed, reverse fault in response to the eastward bend at the southern end of the uplift (Figs. 2 and 3). The stratigraphic separation across this fault together with its topographic expression (sec. 1, T. 21 N., R. 88 W.), indicate that this fault dips steeply to the southeast (Fig. 3). To the east, this fault is manifested by a large bend in strike of the Triassic through Cretaceous stratigraphic section (Barlow, 1953; Fig. 2).

Finally, the inner part of the Rawlins arch is presently a topographic low (i.e., Cherokee Creek valley) that is characterized by poorly exposed, undivided Tertiary sedimentary rocks. A topographic low in the core of the basement-involved, Rawlins uplift is an interesting geomorphic and structural conundrum that was originally recognized by Barlow (1953). In his synthesis of the Rawlins uplift, he postulated a north–south-striking, eastward-dipping normal fault on the west side of Cherokee Creek valley along which rocks east of this fault were displaced downward with respect to rocks west of the fault (i.e., the forelimb of the Rawlins arch). We do not support this interpretation, but conclude that modern Cherokee Creek valley follows a late Tertiary paleovalley localized along a zone of intense brittle fracturing and faulting in the Precambrian basement rocks where preferential erosion occurred. Data in support of our new hypothesis for the origin of the Cherokee Creek valley and its implications for the development of the Rawlins uplift are included later in this article.

STRATIGRAPHIC FRAMEWORK

Table 1 summarizes the nomenclature and thicknesses of the Phanerozoic stratigraphic units in the map area. Thicknesses are derived from field observations and Barlow (1953). In general, they are thinner than typical values determined for these units in nearby areas with less deformation. Although detailed unit descriptions are beyond the scope of this paper, we provide a brief overview of rheological differences that appear to have influenced the nature and magnitude of deformation of the cover rocks. The Paleozoic rocks exposed in the map area are, in general, considered to behave as a competent unit. A notable exception is the thinning observed in the Cambrian Flathead Sandstone across the axial trace of the fold (Fig. 3). This thinning probably was accommodated through bedding-plane slip and ductile deformation within a shale sequence of variable thickness in the upper part of the Flathead Sandstone (Barlow, 1953; Middleton, 1980).

The shaly, and consequently weak, Mesozoic section deformed ductilely during the development of this Laramide uplift. Units in the map area that experienced significant ductile deformation include the Triassic Red Peak and Jelm Formations (the lower and upper units of the Chugwater Group, respectively), Upper Jurassic Morrison Formation, and Lower Cretaceous Thermopolis Shale through Upper Cretaceous Niobrara and Steele Formations (Table 1). Despite a general lack of ductile deformation within the competent Mesozoic units (e.g., Sundance and Cloverly Formations), features such as slickensides on bedding-parallel surfaces in these units are common. The bedding-plane slip in these units is probably directly linked to the magnitude of ductile deformation in the overlying and underlying shaly units.

The dominant Precambrian rock in the map area is a megacrystic, biotite monzogranite. Large (1.5–3 cm), tabular crystals of alkali feldspar and plagioclase locally define a weak magmatic foliation. This granitic basement unit locally contains enclaves of older metamorphic rocks, is cut by scarce mafic dikes, and contains an east–southeast-striking, steeply dipping, 15 m-wide, greenschist-facies shear zone in the NE¼, sec. 34, T. 22 N., R. 88 W. (Fig. 3).

SERIAL CROSS SECTIONS

Introduction

The basic geometry of the Rawlins uplift and the exposed frontal fault zone is illustrated by five cross sections (Fig. 4*A–E*; see cross section lines on Fig. 3). All of the cross sections are at the same scale (albeit different from the geologic map [Fig. 3]), and are roughly northeast–southwest-striking. These serial cross sections are discussed from south (A–A') to north (E–E'). This arrangement provides an opportunity for an approximate down-plunge view of the map area. Thus section A–A' exhibits the greatest displacement (throw) along the frontal fault system, whereas strain decreases to the north (e.g., section E–E') and/or is partitioned into other structural features. Cross section D–D' (Fig. 4*D*) strikes north-northeast–south-southwest, and is at a high angle to the trend of the previously discussed, Lower Triassic-cored parasitic fold.

On the cross sections, bedding thicknesses are shown as measured in the field and maintained separately within the forelimb and backlimb of the uplift. We used this approach because several studies have shown that beds in highly deformed forelimbs of fault-related folds in the Rocky Mountain foreland are commonly thinned (Stearns, 1978; Schmidt and Garihan, 1983; Erslev, 1991; Schmidt et al., 1993; Kellogg et al., 1995). In contrast, beds on the more gently dipping backlimb of such folds are thickened due to up-dip bedding-plane slip and/or out-of-the-syncline faulting.

Borehole data were used in the construction of sections D–D' and E–E' (Figs. 4*D* and *E*; Table 2), and a structure-contour map on the top-of-basement (Blackstone, 1993; Fig. 1) was used as a source for depths to Precambrian basement rocks directly below the frontal fault zone. Blackstone's basement structure-contour map indicates a decrease in vertical separation from south to north along the frontal fault zone. In the southernmost cross section (Fig. 4*A*) the frontal fault has slightly over 6,000 ft (1830 m) of throw. The series of faults in the northernmost cross

Legend for cross sections

Rock units:

Quaternary	Q_{ad}	Quaternary anthropogenically disturbed	
	Q_c	Quaternary colluvium	
	Q_{al}	Quaternary alluvium	
	Q_{ls}	Quaternary landslide deposit and talus	
Tertiary	T_g	Tertiary gravel	
	T_u	Tertiary undifferentiated	
Cretaceous	K_{nbs}	Niobrara Formation and Steele Shale	
	K_f	Frontier Formation	
	K_{my}	Mowry Shale	
	K_{md}	Muddy Sandstone	
	K_t	Thermopolis Shale	
	K_c	Cloverly Formation	
Jurassic	J_m	Morrison Formation	
	J_s	Sundance Formation	
Triassic	TR_j	Jelm Formation	Chugwater Group
	TR_a	Alcova Limestone	Chugwater Group
	TR_{rp}	Red Peak Formation	Chugwater Group
Permian	P_{ge}	Goose Egg Formation	
Pennsylvanian	IP_t	Tensleep Sandstone	
	IP_a	Amsden Formation	
Mississippian	M_m	Madison Limestone	
Cambrian	$Ꞓ_f$	Flathead Sandstone	
Precambrian	pꞒ	Precambrian rocks, undivided	

Figures 4*A–E*. Cross sections A–A' to E–E' across the Rawlins uplift.

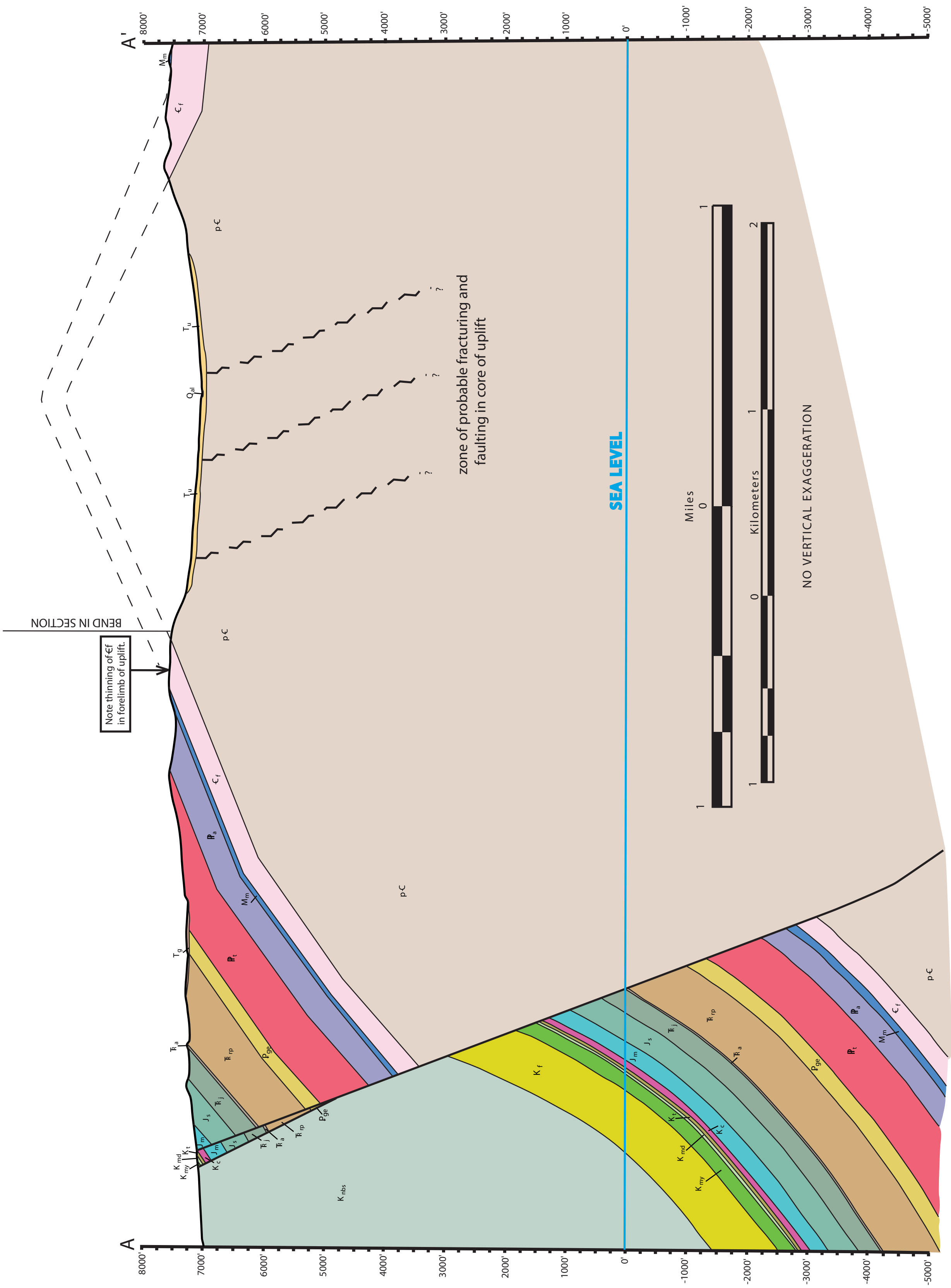
A
A'
8000'
7000'
6000'
5000'
4000'
3000'
2000'
1000'
0'
-1000'
-2000'
-3000'
-4000'
-5000'
SEA LEVEL
zone of probable fracturing and faulting in core of uplift
Note thinning of €f in forelimb of uplift.
BEND IN SECTION
Miles
Kilometers
NO VERTICAL EXAGGERATION
p-C
K nbs
K f

Figure 4A

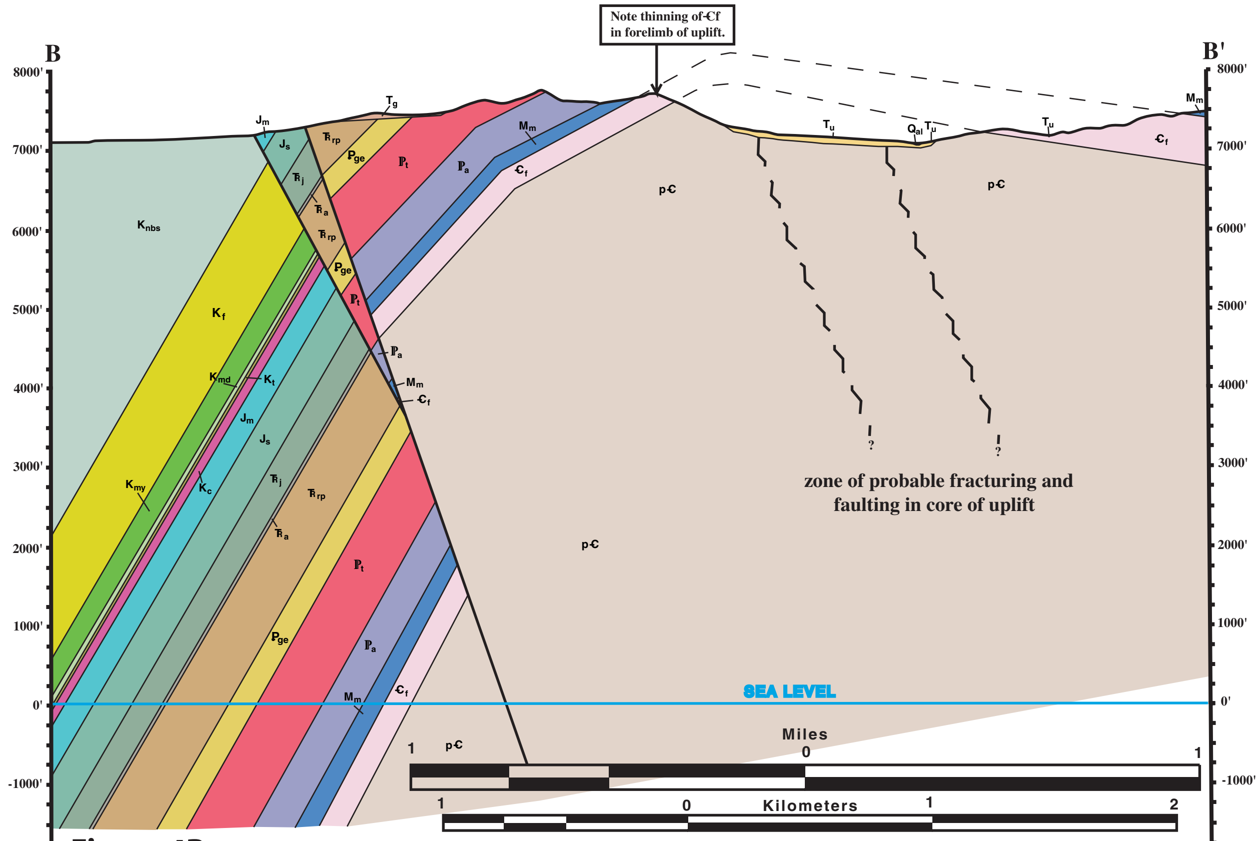

Figure 4B

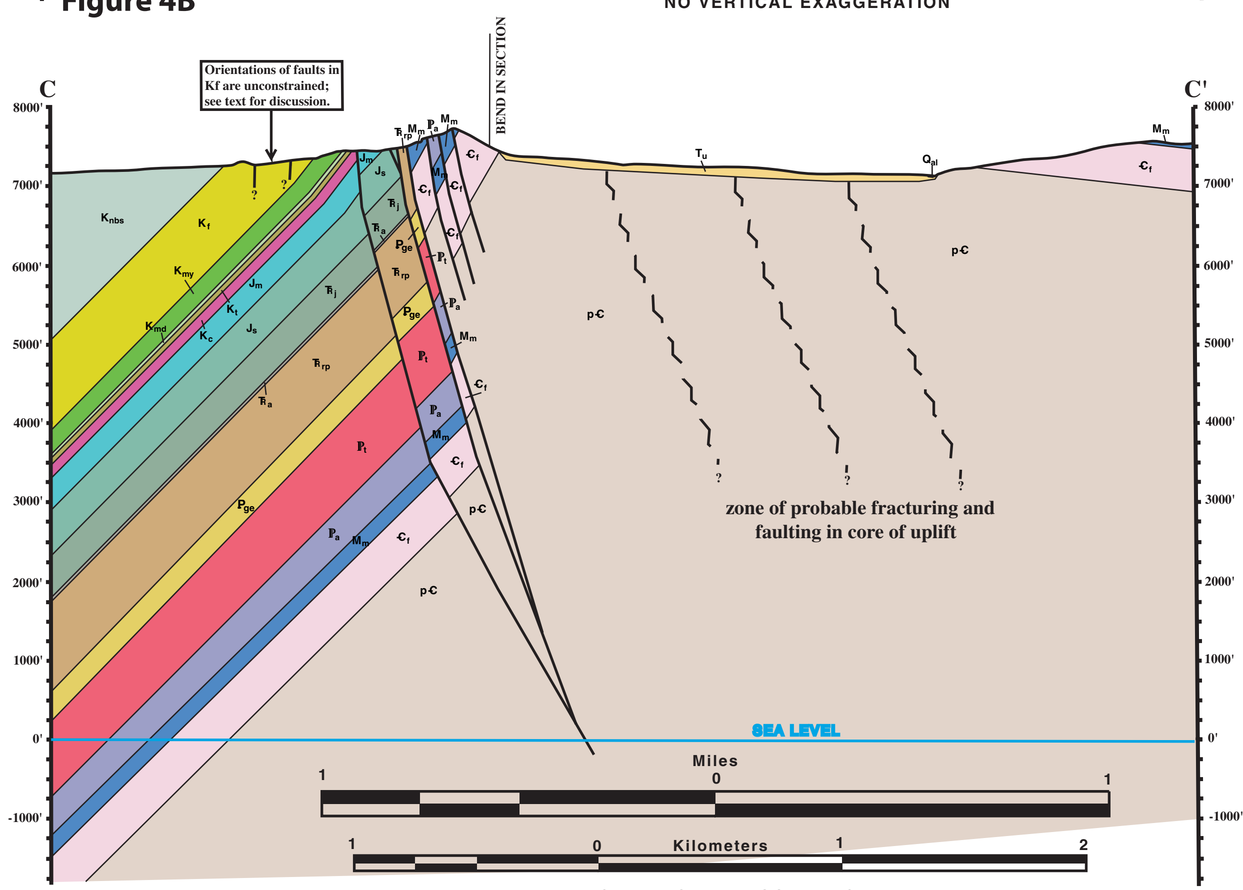

Figure 4C

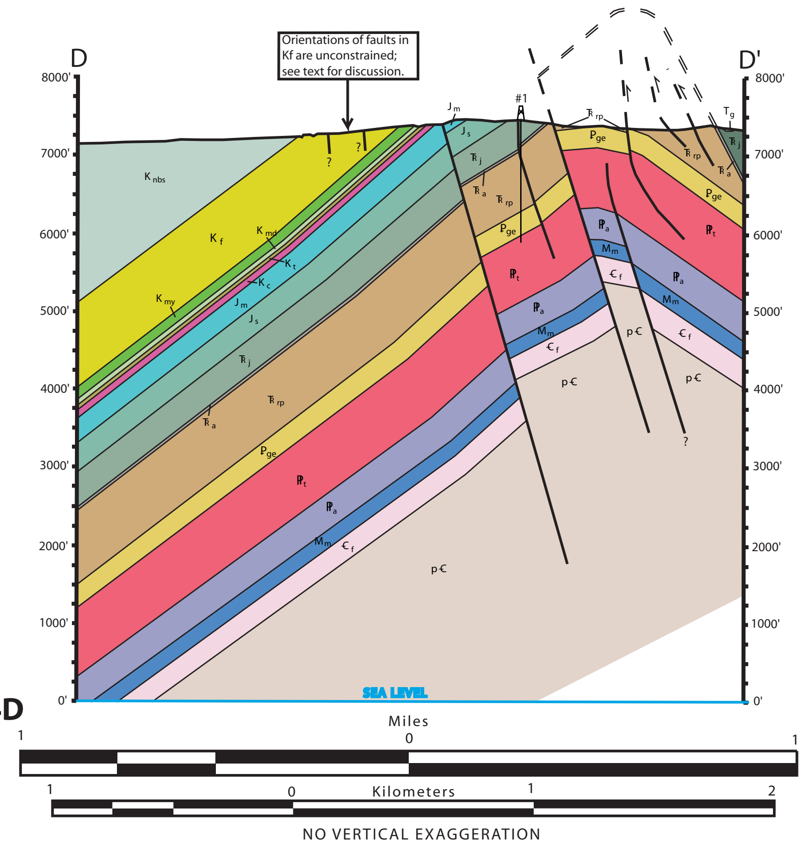

Figure 4D

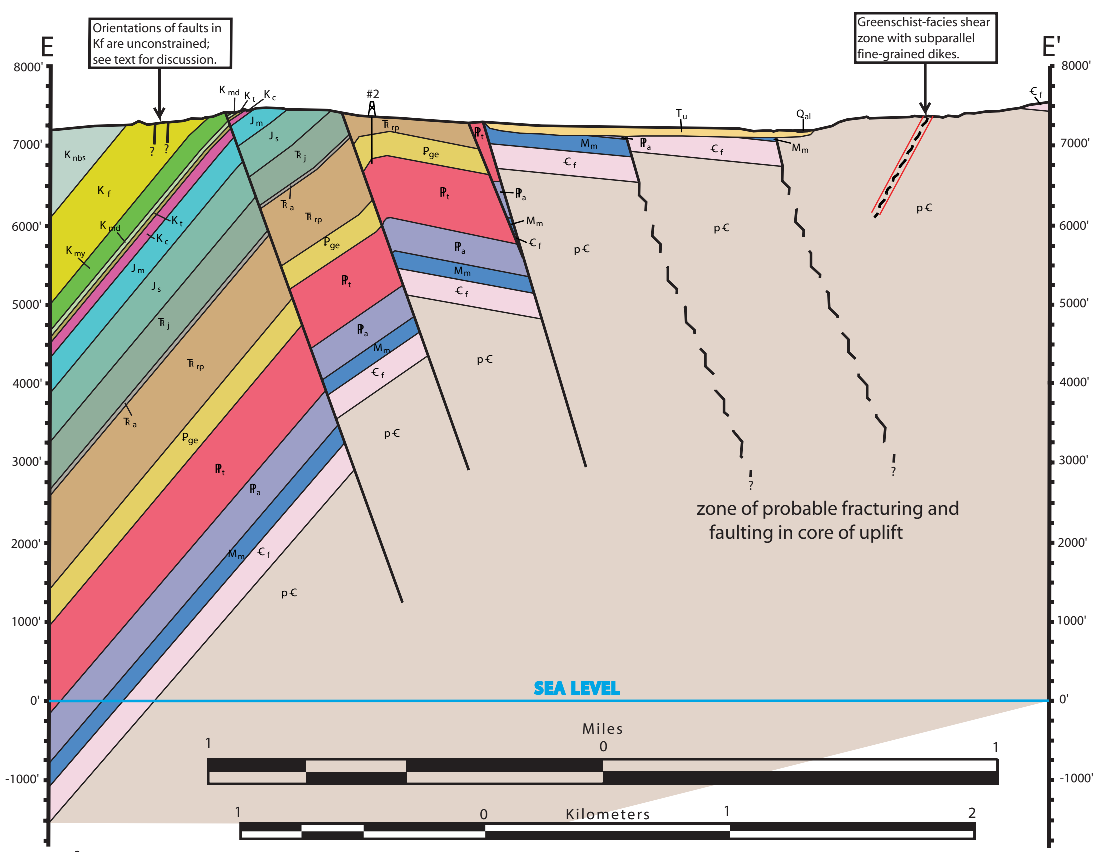

Figure 4E

Table 2. Summary of borehole data used in construction of cross sections D–D' (Fig. 4D) and E–E' (Fig. 4E).

Borehole #1 = API #49-007-05567

Location: SW1/4, NE1/4, sec. 4, T. 21 N., R. 88 W.

Elevation KB: 7,427 ft

Total depth: 1,520 ft

Tops of formations:	Alcova Limestone:	368 ft
	Dinwoody Formation:	1,125 ft
	Goose Egg Formation:	1,181 ft
	Tensleep Sandstone:	1,480 ft

Borehole #2 = API #49-007-05570

Location: NW1/4, NE1/4, sec. 4, T. 21 N., R. 88 W.

Elevation KB: 7,370 ft

Total depth: 665 ft

Tops of formations:	Goose Egg Formation:	325 ft
	Tensleep Sandstone:	525 ft

section (Fig. 4*E*) collectively are interpreted to carry roughly half that throw value.

Cross section A–A'

Cross section A–A' (Fig. 4*A*) displays the maximum amount of throw across the uplift-bounding, frontal fault zone within the map area (Fig. 3). A 70°-dipping fault plane is employed to accommodate a basement depth of approximately 5,000 ft (1525 m) below sea level in the footwall (Fig. 1). Such a steep dip for a basement-involved contractional fault is not uncommon in the upper levels of Rocky Mountain foreland uplifts (e.g., Blackstone, 1940; Brown, 1988, 1993; Stone, 1993a). However, such reverse faults are commonly listric in the subsurface or merge into a low-dipping (~25–30°) thrust-fault zone at depth (Stone, 1993a).

The thickness change in the Cambrian Flathead Sandstone (forelimb versus backlimb) illustrates the degree of thinning that apparently occurred in the forelimb of the Rawlins arch. Flathead thickness in the backlimb of the fold is ~600 ft (~183 m), whereas in the forelimb it is only ~300 ft (~91 m). Another notable feature in this cross section is the geometry of the Precambrian basement rocks. There has been a long-standing debate concerning the mechanical behavior of basement rocks in Laramide arches. One aspect of this debate is focused on the folding of basement rocks (Blackstone, 1983; Brown, 1988, 1993; Schmidt et al., 1993; Kellogg et al., 1995; Bump, 2003). Erslev and Rogers (1993) concluded that basement folding is limited to an area within ~1 km (~.6 mi) of the fault plane in situations where basement is faulted above sedimentary strata along a single fault plane. On the hanging-wall block, folding of the basement–cover unconformity occurs so that the contact is "dragged" toward the fault. An example of this folding of the basement–cover unconformity is shown in Figure 4*A*.

Cross section B–B'

Cross section B–B' (Fig. 4*B*) is similar to section A–A', but they differ in the vertical displacement associated with the frontal fault zone. Section B–B' obliquely transects the fault ramp responsible for the progressive increase in vertical displacement (throw) to the south (Fig. 3). Thus vertical displacement in cross section B–B' is less than the displacement in cross section A–A' (Fig. 4*A*). Another noteworthy aspect of cross section B–B' is the obliquity of the cross section line relative to the strike of bedding and frontal faults. Thus in this cross section the apparent dips of bedding and the fault planes are less than the true dips of these

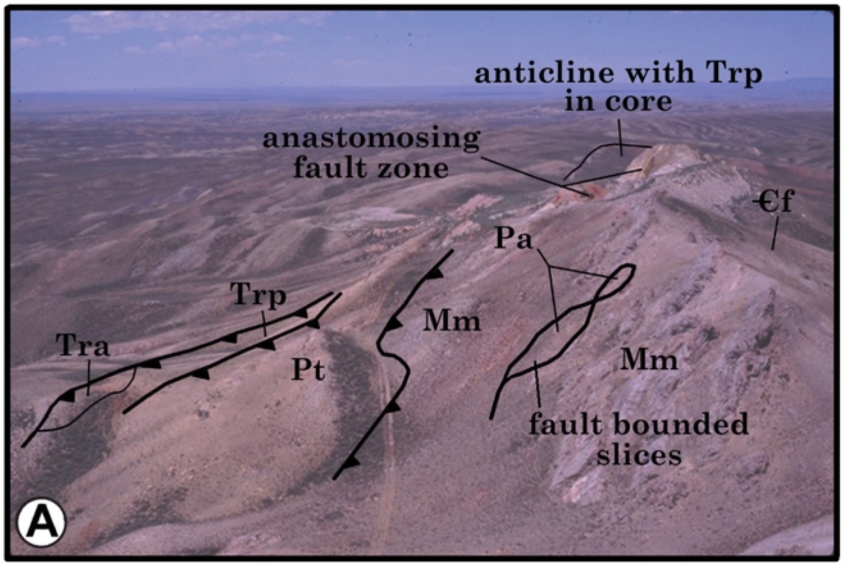

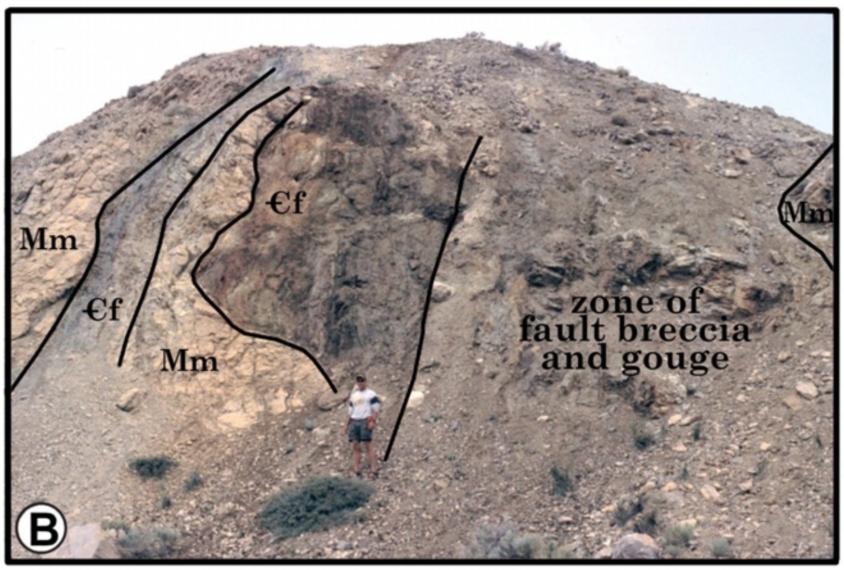

Figure 5. ***A,*** View north from Cherokee Peak of the complex character of faulting along the west flank of the Rawlins uplift (SW¼, sec. 3, T. 21 N., R. 88 W.); and ***B,*** Photograph illustrating anastomosing nature of faults (west-central part of sec. 4, T. 21 N., R. 88 W. looking north). Bedding attitudes at this locality are obscured by concentrated brittle deformation. The zone of breccia and gouge is a mixture of Mississippian Madison Limestone (Mm) and Cambrian Flathead Sandstone (€f).

features in the area transected by the cross section line. Finally, basement folding in the hanging-wall block of cross section B–B' is comparable to the folding of basement rocks in cross section A–A', as indicated by the bend of the basement–cover contact towards the fault plane.

Cross section C–C'

Cross section C–C' transects an anastomosing fault zone (Figs. 4*C* and 5*A*). This area is characterized by slivering of Pennsylvanian and Mississippian strata along subsidiary faults with relatively minor displacement (Figs. 3 and 5*B*). Forelimb dips are comparatively steeper on this cross section. This observation suggests that the basement–cover contact may also be steeply dipping. These steep dips also suggest that discrete fault-bounded basement blocks may have undergone various degrees of rotation within the forelimb of the Rawlins uplift, as illustrated in cross section C–C'. However, because bedding attitudes are commonly obscure where transected by cross section C–C' (Fig. 5*B*), an alternative structural interpretation (not illustrated in cross section C–C') is a decoupling (detachment) zone near the basement–cover contact. Cover rocks above this inferred decoupling zone could have deformed independently from the more rigid basement rocks. Consequently, bedding attitudes in the exposed cover rocks may not parallel or match the orientation of the basement–cover contact in the subsurface.

Cross section D–D'

Cross section D–D' was constructed to investigate the 2-D geometry and character of the Triassic-cored, parasitic anticline previously mentioned, utilizing the subsurface data from borehole #1 (Table 2, Figs. 3 and 4*D*). Because the strike of the cross section line is oriented ~60° to the strike of bedding, beds in the footwall (Fig. 3) actually dip more steeply than shown in Fig. 4*D*. Cross section D–D' illustrates that all the frontal faults exhibit from <50 ft (<15 m) to a maximum of 200 ft (61 m) of vertical separation. A notable feature in the cross section is the mesoscopic fold on the eastern side and its relationship to top-of-basement geometry. Field data indicate that the limbs of this fold dip moderately steeply, and the overall width of the fold is only ~2300 ft (~702 m) (Fig. 3). The relative competency of the granitic rocks comprising the Precambrian basement in the map area is significantly greater than that of the stratified cover rocks. Therefore, the basement–cover contact would not be expected to parallel the fold geometry observed in the Phanerozoic cover rocks, and thus ductile deformation and decoupling (detachment) zones are inferred to occur within this parasitic fold. The locus of this deformation was most likely the weak shales of the Lower Triassic Red Peak Formation. This explanation accounts for the thickening of the Red Peak Formation on the east limb of the fold as well as the repeated small thrust offsets observed in the outcrop pattern of the Alcova Limestone (Fig. 3).

Cross section E–E'

Cross section E–E' transects the parasitic anticline where the Lower Triassic Red Peak Formation crops out (Fig. 4*E*). This cross section also passes through borehole #2, which provided data for stratigraphic tops of the Permian Goose Egg Formation and Pennsylvanian Tensleep Sandstone (Table 2). On cross section E–E', a fault truncates the anticline on its eastern flank or limb at a high angle, as indicated by the straight trace of the contact across an area of topographic relief (Fig. 3). Although Barlow (1953) also mapped this contact, it is hard to envision a fault-bounded block of Pennsylvanian Tensleep Sandstone (SE¼, sec. 33, T. 22 N., R. 88 W.) juxtaposed with the Triassic-cored anticline by a fault with normal-sense displacement. This geometric conundrum is a key factor in concluding that a normal fault does not bound the west side of Cherokee Creek valley. Furthermore, given the present topography of the Cherokee Creek valley, it is possible that numerous basement faults occur in the core of the Rawlins uplift and were subsequently buried by late Tertiary strata (Fig. 4*E*). According to this interpretation, modern Cherokee Creek valley follows a late Tertiary paleovalley that developed during preferential erosion of the fractured and faulted(?) inner part of the Rawlins uplift. Furthermore, the map distribution of the lower Mesozoic and upper Paleozoic units on the east side of the anticline (Fig. 3) indicates that the basement–cover unconformity must dip eastward; i.e., it is part of the backlimb of the Rawlins arch. These relationships also suggest that there may be buried, basement-involved faults in the Cherokee Creek valley along which the Cambrian Flathead Sandstone was uplifted to its present position on the backlimb of the fold near E' (Fig. 4*E*).

SUBSURFACE DATA AND FEATURES

Only two boreholes with formational marker information exist within the map area (Table 2), and both are located in the NE¼, sec. 4, T. 21 N., R. 88 W. (Figs. 3 and 4*D, E*). Borehole #1, the deeper of the two, penetrated the Pennsylvanian Tensleep Sandstone at a depth of 1,480 ft (451 m) and reached a total depth of 1,520 ft (464 m) (Table 2). Borehole #2 penetrated the Pennsylvanian Tensleep Sandstone at a depth of 525 ft (160 m) and reached a total depth of 665 ft (203 m).

A seismic-reflection profile (Line SPL-2, Fig. 6) was obtained from Seismic Exchange, Inc. (SEI) for use in this study. This profile is not depth migrated; consequently, the positions of bedding reflectors and faults require adjustment to determine their true position in the profile. The position of Line SPL-2 is approximately located on Figure 3.

Seismic-reflection profile, SPL-2, was acquired in the early 1980s and processed in 1984. Image quality in this profile is poor, but the line provides evidence for interpretation of the master fault zone at depth (Fig. 6). The profile was converted to 1:1 scale to eliminate an original vertical exaggeration (i.e., scaled such that dipping reflectors near the top of image are coincident with attitudes measured in outcrop; Stone, 1991). However, this does not account for the possible foreshortening at depth resulting from the high velocity of seismic energy through the basement rocks. Digital files of the seismic data were not available, so it was necessary to estimate depth, using velocities typical for the rock types imaged along the profile. Christensen and Mooney (1995) compiled a range of velocities for numerous rock types according to depth. Using an average velocity of 20,270 ft/s (6.182 km/s) (Christensen and Mooney, 1995) for granite at ~16,394 ft (5 km) depth, we approximated depth to the fault zone in the core of the uplift (Fig.

6*B*). This process was repeated east of the core of the uplift. However, in this calculation, a thin veneer of Phanerozoic sedimentary strata was taken into account. Using a velocity of 14,755 ft/s (4.5 km/s) (Christensen, 1982) for the sedimentary sequence, and then applying the 20,270 ft/s (6.182 km/s) to the granitic basement rock, we determined a second depth to the fault zone. The horizontal scale of the seismic-reflection profile is known. Therefore, by using the difference between the two estimated depths, a simple arc-tangent ("rise-over-run") calculation was used to estimate the dip of the fault zone. This calculation yielded a dip of ~23°, a difference of ~3° from the apparent 20° dip of the fault surface in the seismic-reflection profile (Fig. 6*B*). It is important to note that the fault surface on which the dip calculation was made is part of an anastomosing, braided fault zone (Figs. 6 and 7). Figure 7 is an expanded view of the region outlined in Figure 6*A* and illustrates the seismic-reflection character and basic geometry of the low-angle, braided fault zone interpreted in Figure 6*B* at depth. Individual faults mapped at the surface do not exhibit the amount of slip necessary to account for the net structural relief on the basement–cover contact between the core of the uplift and the adjacent basins. These faults are interpreted as splays off a shallowly dipping, braided, master fault zone (Figs. 6 and 7) with a cumulative slip history that presumably can account for the overall structural relief of the Rawlins uplift.

DISCUSSION

Fault Geometries

Fault orientations within the map area dominantly strike northwest–southeast (Fig. 3). The exceptions to this observation are the three cross-faults on the east side of the map area, the north–south lineament of the major frontal reverse fault (fault ramp in secs. 10 and 15, T. 21 N., R. 88 W., Fig. 3), and the prominent eastward bend of the same fault at the southern margin of the map area (Figs. 1 and 2). This basic fault geometry implies dominantly southwest–northeast shortening during the development of the Rawlins uplift.

The western part of the map area can basically be considered a broad fault zone. Sections 3 and 4, T. 21 N., R. 88 W. especially provide insight into the complexity of faulting within the Rawlins uplift (Figs. 3 and 5). Faults within this area display an anastomosing geometry, commonly juxtaposing normally adjacent units in an almost random order. Due to the scale of his mapping, Barlow (1953) did not document the anastomosing/splaying character of the faults at the surface within the uplift. The slicing and slivering nature of these faults has effectively obscured much of the original bedding. Consequently, reliable structural attitudes are sparse within this area. At many localities, faults may be recognized only by a change in formational thickness or by the absence of otherwise distinctive strata of a formation. The two sub-parallel faults within the Cretaceous Frontier Formation along the forelimb are a good example of this phenomenon (Fig. 4*C, D*). In the northern part of the map area, the Frontier Formation includes three distinct sandstone units, each of which forms a prominent ridge (SE¼, sec. 32, T. 22 N., R. 88 W.; Fig. 3). The stratigraphically highest sandstone unit is the Wall Creek Member, and only this sandstone is continuous to the south. The two lower sandstones are generally absent. Thus, it is on the basis of these missing sandstone units that the two sub-parallel faults are inferred (Fig. 3). Due to the fact that these inferred faults are in shaly units, fault orientation and sense of displacement are uncertain. Consequently, the traces of the faults are dashed on the geologic map (Fig. 3). The general absence of the prominent sandstone units along the outcrop suggests a normal-sense of displacement along these faults (i.e., thinning the stratigraphic section by the "cutting-out" of units).

Fold-out figures on pages 80-81

Page 80
Figure 6. Unmigrated seismic-reflection profile SPL-2. Vertical scale is two-way time in seconds. ***A,*** Uninterpreted profile with the area of Figure 7 outlined; and ***B,*** Interpreted profile.

Page 81
Figure 7. Expanded view of the region outlined in Figure 6*A*, illustrating the seismic-reflection character and geometry of the low-angle, braided fault zone interpreted in Figure 6*B* at depth.

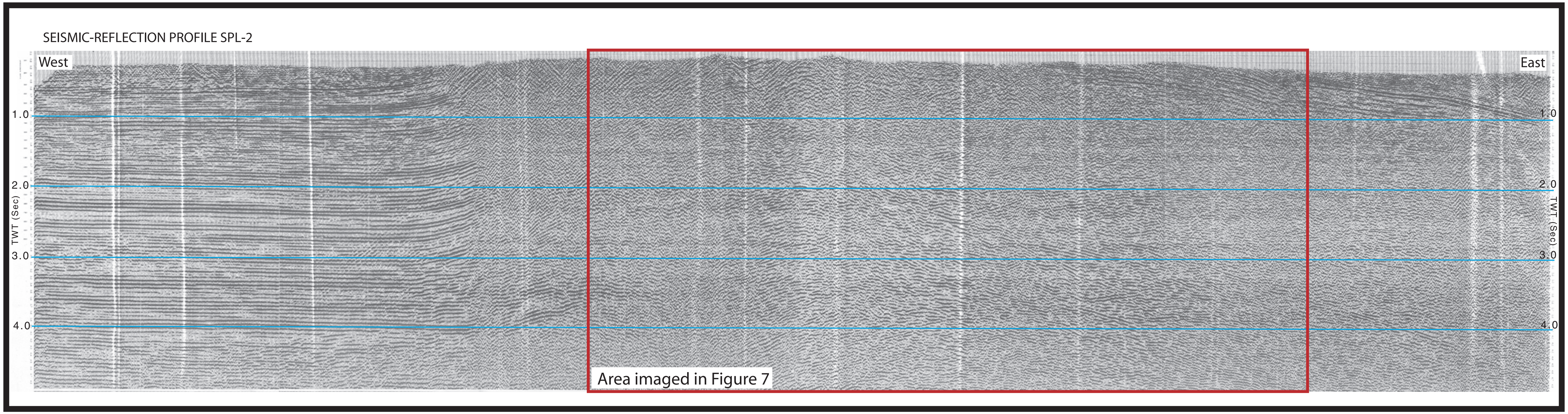

Figure 6A

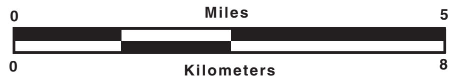

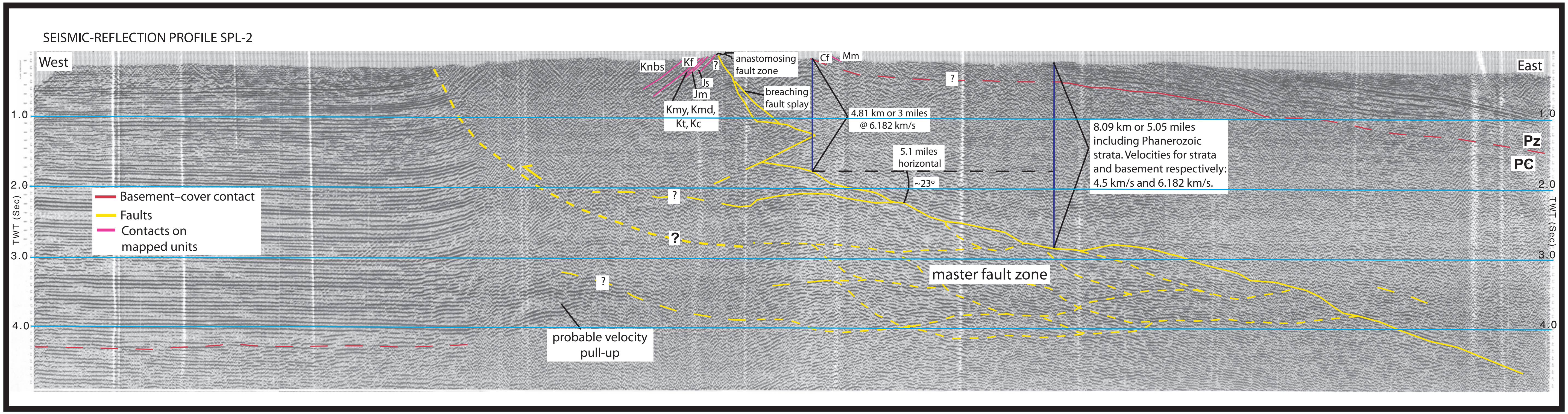

Figure 6B

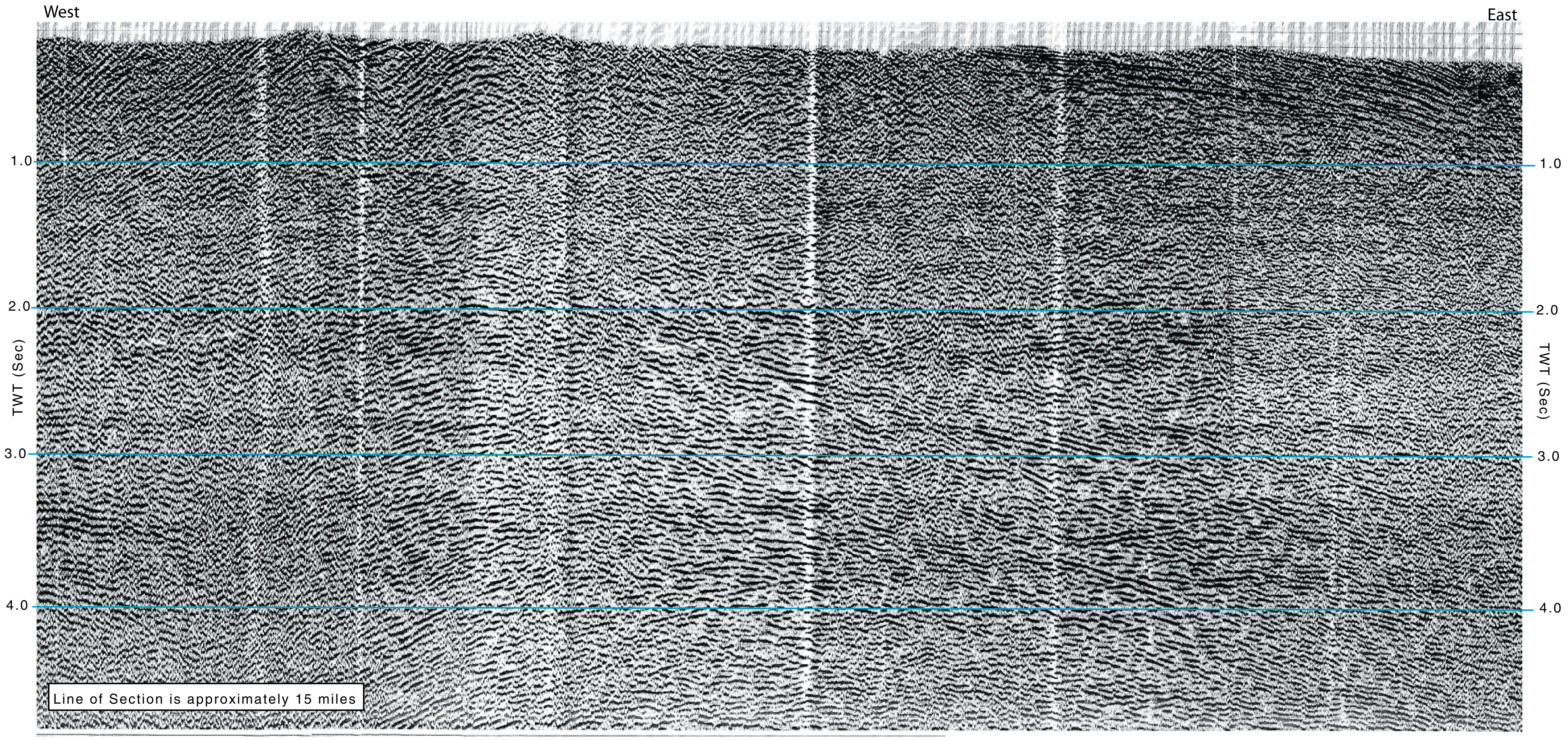
West
East
1.0
2.0
3.0
4.0
TWT (Sec)
1.0
2.0
3.0
4.0
TWT (Sec)
Line of Section is approximately 15 miles

Figure 7

We suggest that the aforementioned fault ramp and major cross-fault (sec. 1, T. 21 N., R. 88. W.) are kinematically related to the eastward bend of the bounding fault-zone trace at the southern end of the uplift. This prominent change in structural trend can be traced ~21 mi (~34 km) to the east, at least to south of Walcott Junction (Rocky Mountain Map Company, 1992; Fig. 1). This structural trend marks the boundary between the Rawlins uplift and the north-plunging Hatfield anticline (Fig. 1). In addition, the Grenville dome, a doubly plunging, elliptical anticline with the long axis extending east–west, is localized directly along this trend (Fig. 2; Jenkins, 1951; Barlow, 1953).

We interpret this prominent bend in structural trend as a manifestation of a pre-existing crustal anisotropy or discontinuity in the Precambrian basement rocks. That interpretation is based on the observation that this orientation is parallel to the strike of the late Mesoproterozoic–Neoproterozoic, east–west Uinta trend (Bryant, 1985; Stone, 1993b). This east–west strike is sub-parallel to the primary local shortening direction, implying an important component of sinistral, oblique-slip displacement along this structural trend.

If some inhibitor to west-directed, reverse-sense displacement was present across this east–west-striking structure (e.g., an extension of the north-plunging Hatfield anticline), such a buttress could impede fault slip at the southwest corner of the uplift. Therefore, some other volumetric adjustment mechanism would be necessary to accommodate strain. We propose that the major cross-fault (sec. 1, T. 21 N., R. 88 W.) is the evidence for the partitioning of that strain into another structural feature. This fault dips steeply to the southeast as indicated by its topographic expression (Fig. 3). Its geometry suggests that the fault is a back-thrust to the north-dipping, east–west-striking discontinuity along the southern margin of the Rawlins uplift. We believe that the basement block between the back-thrust and north–south-striking primary fault zone arose in response to some slip inhibitor along the east–west-striking discontinuity. In turn, this inhibitor also facilitated the ramp-up through the stratigraphic section in the southwestern corner of the map area (Fig. 3). This interpretation is supported by the important observation, based on the basement structural configuration map (Fig. 1) and the serial cross sections (Fig. 4), that the greatest vertical displacement occurs along the southwest margin of the uplift. These fundamental relationships imply that structures within the map area were not synchronous in their development, but occurred in the following chronology: (1) general west-directed displacement of the basement block (i.e., uplift as a whole), (2) inhibition of fault slip along east–west-striking, basement-rooted discontinuity, and (3) contemporaneous back-thrusting along cross-fault and synchronous ramping through the stratigraphic section along the frontal fault zone.

Subsurface fault geometries are difficult to interpret. The seismic-reflection profile SPL-2 provides a poor image of the fault zone at depth (Fig. 6). However, it does suggest two things. First, the frontal faults in the map area comprise subsidiary splays off a master fault zone at depth with a shallow dip (~25°) to the east. Second, this fault zone has an anastomosing, braided character defined by fault-bounded, lenticular slices of basement rocks—a geometry also suggested by Sharry et al. (1986) for the deep structure of the Wind River thrust. In light of these conclusions on the geometry of the fault system responsible for the development of the Rawlins uplift, the master fault zone at depth dips ~25° (Fig. 6) but high-angle (~70°) splays off this system define the frontal faults exposed at the Earth's surface (Figs. 3 and 4).

Folding and Block Rotation

Folding of the sedimentary cover above basement uplifts or arches is typically well developed, and has been studied by many workers (e.g., Schmidt and Garihan, 1983; Erslev, 1991; Erslev and Rogers, 1993; Schmidt et al., 1993; Stone, 1993a; 2002; Bump, 2003). Commonly, folding of the sedimentary cover has been accompanied by thinning of stratigraphic units in the forelimb of the fold and thickening of these in the synclinal hinge (e.g., Schmidt and Garihan, 1983; Stone, 1984, 1993a; Brown, 1988, 1993; Erslev, 1991; Schmidt et al., 1993; Kellogg et al., 1995). A fundamental problem in the analysis of basement-involved uplifts is the mechanical response of the generally strong Precambrian basement rocks during contraction; i.e., do the basement rocks fold, fault, or do both? The purpose of this discussion is not to address the general question, but to offer an interpretation specific to the Rawlins arch. Within the map area, sedimentary units on the forelimb

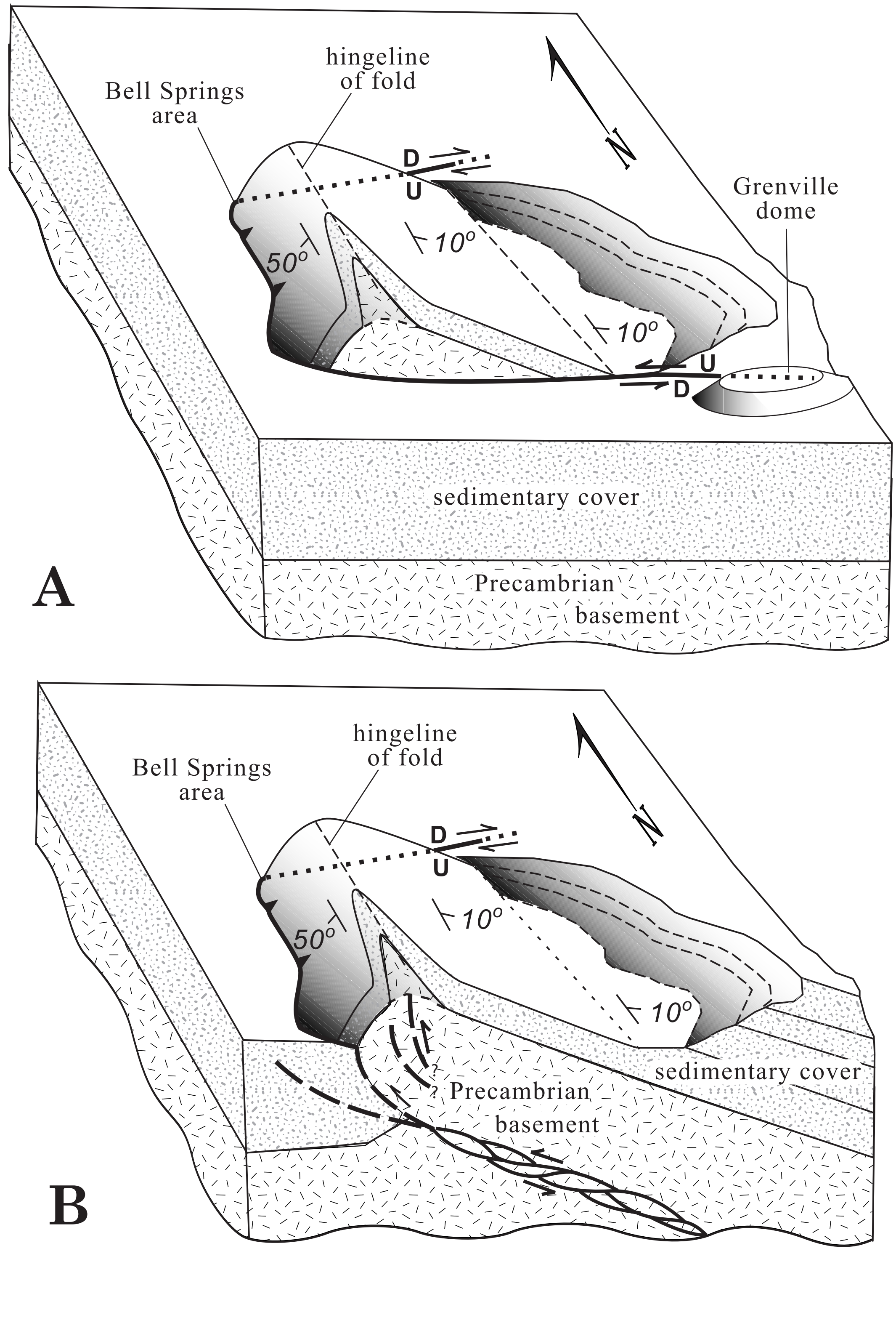

Figure 8. Three-dimensional, schematic diagrams of Rawlins uplift. ***A,*** View to northwest showing general surface geometry of uplift and associated structural features. ***B,*** Cross sectional view along southern margin of uplift illustrating kinematic interpretation of relationship between frontal fault(s) and seismically imaged, low-angle, braided, plastic-to-brittle shear zone.

of the fold exhibit significant thinning (e.g., the Flathead Sandstone; Figs. 4*A, B*). However, at other localities in the map area, there is little thinning of the Flathead Sandstone (e.g., Fig. 4*C*). If fracturing and faulting are present in the core of the arch, then it is plausible that the sedimentary units were rotated passively on discrete fault-bounded basement blocks. Folding and block rotation represent two end-members in the spectrum of basement-arch deformation. Certainly some amount of folding of basement is required in the map area to explain the thinning of the Flathead Sandstone (Figs. 4*A, B*). However, rotation of fault-bound, basement blocks is required in the parasitic anticline with a core of incompetent Red Peak Formation (Figs. 4*D, E*).

CONCLUSIONS RELATED TO THE DEVELOPMENT OF THE RAWLINS UPLIFT

The Rawlins uplift is a Laramide, basement-involved, antiformal structure with significant structural relief on the basement–cover contact. The overall geometry of the uplift is that of an asymmetric arch, with a steeply west-dipping forelimb and a gently, homoclinally, east-dipping backlimb (Fig. 8). The north-northwest–south-southeast trend of the uplift suggests a dominantly northeast–southwest shortening axis. The uplift is bounded on its southern and northern ends by eastward bends in the fault system. These abrupt changes in fault orientation are probably due to the influence of pre-existing crustal anisotropies or discontinuities within Precambrian basement rocks.

Vertical relief on the basement–cover unconformity, between the core of the uplift and the basins to the east and west, is ~37,000 ft (~11,285 m) and ~27,000 ft (~8,235 m), respectively. Most of the vertical displacement occurs along a subsurface low-angle fault zone. This thrust-fault zone dips gently to the east and exhibits a braided geometry within the Precambrian basement rocks based on the interpretation of a seismic-reflection profile. The frontal (breaching) faults in the study area are subsidiary, reverse faults that splay off of the master thrust-fault system. Maximum displacement along a discrete reverse fault is only ~6000 vertical ft (~1830 vertical m) at the southwestern corner of the uplift. Progressing northward, displacement along the primary reverse fault decreases, and deformation occurs along a much broader zone of faulting.

Folding and block rotation are common modes of deformation associated with Rocky Mountain foreland uplifts (arches). The Rawlins uplift exhibits characteristics of both modes. At the southwestern corner of the uplift, basement deformation in the hanging-wall block is characterized by folding of the basement–cover contact ~20° toward the fault. In contrast, basement deformation in the northern part of the map area is characterized by rotation of discrete, fault-bounded basement blocks. The difference in character of deformation from south to north is a result of: (1) net vertical displacement, and (2) the change from displacement along a discrete fault plane to distributed displacement within a broader fault zone.

Parasitic folds, superimposed upon the macroscopic fold of the uplift, are present within northern parts of the map area. The most prominent is an anticline detached within the ductile shaly rocks of the Lower Triassic Red Peak Formation. Additional minor anticlines and synclines just northwest of this structure are a result of fault-related undulations in the relatively incompetent rocks of the involved formations.

Buried structures probably exist within the map area. Cherokee Creek valley is located parallel to the axial trace of the uplift (arch). Because the Rawlins uplift has a core of highly competent Precambrian basement rocks, a topographic depression would not be expected along the axial trace of the fold. Barlow (1953) accounted for the valley by postulating a late Tertiary, normal fault along its western side, with a down-to-the-east sense of displacement. However, we found no field evidence to support this interpretation, and our serial cross sections clearly preclude significant normal faulting in the core of the Rawlins uplift. It is more probable that brittle fracturing and faulting of the uplift's core during Laramide deformation led to increased erosion along the axial trace of the fold during Cenozoic time.

SOME REGIONAL IMPLICATIONS AND A POSSIBLE FUTURE STUDY

The basement deformation associated with the Rawlins uplift is characterized by the development of a low-angle, anastomosing, braided fault zone within

Precambrian igneous and metamorphic rocks. This is a previously unrecognized structural style within the greater Hanna Basin region, although a similar subsurface fault-zone geometry was reported by Sharry et al. (1986) for the Wind River thrust. Because the basement fault zone dips shallowly eastward, it is probable that most of the vertical relief was achieved through progressive contractional faulting deep within the Precambrian basement complex. Basement deformation closer to the basement–cover unconformity exhibits a spectrum of behavior, defined by the folding and rotation of discrete, fault-bounded blocks.

This study is geographically limited due to the scale of the geologic mapping. As a result, it does not offer insight into the modes of deformation farther west in the Great Divide Basin such as synclinal crowding, which can result in out-of-the-basin faulting and the development of a basement-involved triangle zone (Erslev, 1991; Erslev and Rogers, 1993; Bump, 2003; Lillegraven et al., 2004; Lageson and Costa, 2004). A regional seismic-reflection profile across the Greater Green River Basin analyzed by Garing and Tainter (1985) indicates considerable structural complexity at the nose of the Hatfield anticline (Fig. 1), where this north-plunging fold interacts with the southern margin of the Rawlins uplift. At this important juncture, the north-plunging Hatfield anticline (Fig. 1) is in direct contact with the southwest-directed Rawlins uplift. Thus, a continuation of this study south as well as west would provide an improved understanding of the relationship between the development of the basement-involved Rawlins arch, Hatfield anticline, and deformation in the southeastern corner of the Great Divide Basin. Furthermore, detailed study of the physical stratigraphy and paleontology of Upper Cretaceous and Lower Tertiary rocks in the Great Divide Basin should provide useful information on the timing of events in the structural development of the Rawlins uplift (arch) and Hatfield anticline.

ACKNOWLEDGMENTS

This article is based on a master's thesis completed at the University of Wyoming by Otteman in 2003; Snoke served as supervisor of the project. The authors thank Jason A. Lillegraven who served on the thesis committee and whose keen interest and knowledge of the Laramide orogeny within the greater Hanna Basin has been an enormous asset in this and similar studies during the past decade. Patricia J. S. Colberg also served on the thesis committee and provided an insightful review of the thesis manuscript. Phyllis A. Ranz of the Wyoming State Geological Survey greatly assisted us in the preparation of the figures for this article. Similarly, we thank Brian P. Kraatz for his initial work on the digital topographic base map for Figure 3. Financial support for this study was made possible by NSF research grant EAR-9909354, awarded to Jason A. Lillegraven and Arthur W. Snoke, and by graduate assistantships through the Department of Geology and Geophysics, University of Wyoming. The seismic-reflection profile (Line SPL-2) used in this study was obtained from Seismic Exchange, Inc. (SEI). Donald S. Stone and Karl S. Kellogg provided exceptionally thorough and helpful reviews of an early version of the manuscript, whereas Donald W. Boyd did a final edit of our manuscript.

REFERENCES CITED

Barlow, J. A., 1953, The geology of the Rawlins uplift, Carbon County, Wyoming: [Ph.D. dissert.]: Laramie, University of Wyoming, 179 p.

Blackstone, D. L., Jr., 1940, Structure of the Pryor Mountains, Montana: Journal of Geology, v. 48, p. 590–618.

______1983, Laramide compressional tectonics, southeastern Wyoming: Contributions to Geology, University of Wyoming, v. 22, p. 1–38.

______1993, Precambrian basement map of Wyoming: Outcrop and structural configuration: Wyoming State Geological Survey Map Series 43, scale 1:1,000,000.

Brown, W. G., 1988, Deformational style of Laramide uplifts in the Wyoming foreland, *in* Schmidt, C. J., and Perry, W. J., Jr., eds., Interaction of the Rocky Mountain foreland and the Cordilleran thrust belt: Boulder, Colorado, Geological Society of America Memoir 171, p. 1–25

______1993, Structural style of Laramide basement-cored uplifts and associated folds, *in* Snoke, A. W., Steidtmann, J. R., and Roberts, S. M. eds., Geology of Wyoming: Geological Survey of Wyoming Memoir No. 5, p. 312–371.

Bryant, B., 1985, Structural ancestry of the Uinta Mountains, *in* Picard, M. D., ed., Geology and energy resources, Uinta Basin of Utah: Salt Lake City, Utah Geological Association Publication, p. 115–120.

Bump, A. P., 2003, Reactivation, trishear modeling, and folded basement in Laramide uplifts: Implications for the origins of intra-continental faults: GSA Today, v. 13, p. 4–10.

Chamberlain, K. R., Frost, C. D., and Frost, B. R., 2003, Early Archean to Mesoproterozoic evolution of the Wyoming Province: Archean origins to modern lithospheric architecture: Canadian Journal of Earth Sciences, v. 40, p. 1357–1374.

Chase, R. B., Schmidt, C. J., and Genovese, P. W., 1993, Influence of Precambrian rock compositions and fabrics on the development of Rocky Mountain foreland folds *in* Schmidt, C. J., Chase, R. B., and Erslev, E. A., eds., Laramide basement deformation in the Rocky Mountain foreland of the western United States: Boulder, Colorado, Geological Society of America Special Paper 280, p. 45–72.

Christensen, N. I., and Mooney, W. D., 1995, Seismic velocity structure and composition of the continental crust: A global view: Journal of Geophysical Research, v. 100, p. 9761–9788.

Christensen, N. I., 1982, Seismic velocities, *in* Carmichael, R. S., ed., Handbook of physical properties of rocks – Volume II: Boca Raton, Florida, CRC Press, p. 1–228.

DeCelles, P. G., Gray, M. B., Ridgway, K. D., Cole, R. B., Srivastava, P., Pequera, N., and Pivnik, D. A., 1991, Kinematic history of a foreland uplift from Paleocene synorogenic conglomerate, Beartooth Range, Wyoming and Montana: Geological Society of America Bulletin, v. 103, p. 1458–1475.

Dobbin, C. E., Hoots, H. W., and Dane, C. H., 1928, Geology and oil and gas possibilities of the Bell Springs district, Carbon County, Wyoming: U.S. Geological Survey Bulletin 796–D, p. 171–201.

Duebendorfer, E. M., and Houston, R. S., 1987, Proterozoic accretionary tectonics at the southern margin of the Archean Wyoming craton: Geological Society of America Bulletin, v. 98, p. 554–568.

Erslev, E. A., 1991, Trishear fault-propagation folding: Geology, v. 19, p. 617–620.

Erslev, E. A., and Rogers, J. L. 1993, Basement-cover geometry of Laramide fault-propagation folds, *in* Schmidt, C. J., Chase, R. B., and Erslev, E. A., eds., Laramide basement deformation in the Rocky Mountain foreland of the western United States: Geological Society of America Special Paper 280, p. 125–146.

Evans, J. P., 1993, Deformation mechanisms and kinematics of a crystalline-cored thrust sheet: The EA thrust system, Wyoming, *in* Schmidt, C. J., Chase, R. B., and Erslev, E. A., eds., Laramide basement deformation in the Rocky Mountain foreland of the western United States: Geological Society of America Special Paper 280, p. 147–161.

Garing, J. D., and Tainter, P. A., 1985, Greater Green River Basin regional seismic line, *in* Gries, R. R., and Dyer, R. C., eds., Seismic exploration of the Rocky Mountain region: Denver, Colorado, Rocky Mountain Association of Geologists and Denver Geophysical Society, p. 233–238

Hoppin, R. A., 1961, Precambrian rocks and their relationship to Laramide structure along the east flank of the Bighorn Mountains near Buffalo, Wyoming: Geological Society of America Bulletin, v. 72, p. 351–368.

Hoy, R. G., and Ridgway, K. D., 1997, Structural and sedimentological development of footwall growth synclines along an intraforeland uplift, east-central Bighorn Mountains, Wyoming: Geological Society of America Bulletin, v. 109, p. 915–935.

Jenkins, C. E., 1951, Grenville dome, Carbon County, Wyoming, *in* Sixth Annual Field Conference, South Central Wyoming: Casper, Wyoming Geological Association Guidebook, p. 58–59.

Kellogg, K. S., Schmidt, C. J., and Young, S. W., 1995, Basement and cover-rock deformation during Laramide contraction in the northern Madison Range (Montana) and its influence on Cenozoic basin deformation: American Association of Petroleum Geologists Bulletin, v. 79, p. 1117–1137.

Lageson, D. R., and Costa, C. H., 2004, Laramide-style backthrusts and triangle zones in the U.S. Rockies and Sierras Pampeanas, Argentina: Geological Society of America Abstracts with Programs, v. 36, no. 5, p. 267.

Lillegraven, J. A., Snoke, A. W., and McKenna, M. C., 2004, Tectonic and paleogeographic implications of late Laramide geologic history in the northeastern corner of Wyoming's Hanna Basin: Rocky Mountain Geology, v. 39, p. 7–64.

McConnell, D. A., and Wilson, T. G., 1993, Linkage between deformation of basement rocks and sedimentary rocks in basement-involved foreland folds, *in* Schmidt, C. J., Chase, R. B., and Erslev, E. A., eds., Laramide basement deformation in the Rocky Mountain foreland of the western United States: Geological Society of America Special Paper 280, p. 319–333.

Middleton, L. T., 1980, Middle Cambrian Flathead Sandstone, [Ph.D. dissert.]: Laramie, University of Wyoming, 182 p.

Mitra, G., 1984, Brittle to ductile transition due to large strains along the White Rock thrust, Wind River Mountains, Wyoming: Journal of Structural Geology, v. 6, p. 51–61.

Molzer, P. C., and Erslev, E. A., 1995, Oblique convergence during northeast-southwest Laramide compression along the east-west Owl Creek and Casper Mountain arches, central Wyoming: American Association of Petroleum Geologists Bulletin, v. 79, p. 1377–1394.

Narr, W., and Suppe, J., 1994, Kinematics of basement-involved compressive structures: American Journal of Science, v. 294, p. 802–860.

O'Connell, P. J., 1996, Kinematics of the eastern flank of the Beartooth Mountains, Montana and Wyoming, *in* Bowen, C. E., Kirkwood, S. C., and Miller, T. S., eds., Resources of the Bighorn Basin: Casper, Wyoming Geological Association, 47th Field Conference Guidebook, p. 189–220.

Ray, R. R., and Berg, C. R., 1985, Seismic interpretation of the Casper arch thrust, Tepee Flats field, Wyoming, *in* Gries, R., and Dyer, R. C., eds., Seismic exploration of the Rocky Mountain region: Denver, Colorado, Rocky Mountain Association of Geologists and Denver Geophysical Society, p. 51–58.

Resor, P. G., and Snoke, A. W., 2005, Laramie Peak shear system, central Laramie Mountains, Wyoming, USA: regeneration of the Archean Wyoming province during Paleoproterozoic accretion, *in* Bruhn, D., and Burlini, L., eds., High-strain zones: Structure and physical properties: London, Geological Society Special Publication 245, p. 81–107.

Rocky Mountain Map Company, 1992, Structure contour map of the Hanna Basin, Wyoming (revised 2002): Casper, Wyoming, Barlow & Haun, Inc., scale 1 inch = 2 miles, 1 sheet.

Schmidt, C. J., and Garihan, J. M., 1983, Laramide tectonic development of the Rocky Mountain foreland of southwestern Montana, *in* Lowell, J. D., and Gries, R., eds., Rocky Mountain foreland basins and uplifts: Denver, Colorado, Rocky Mountain Association of Geologists, p. 271–294.

Schmidt, C. J., Genovese, P. W., and Chase, R. B., 1993, Role of basement fabric and cover-rock lithology on the geometry and kinematics of twelve folds in the Rocky Mountain foreland, *in* Schmidt, C. J., Chase, R. B., and Erslev, E. A., eds., Laramide basement deformation in the Rocky Mountain foreland of the western United States: Boulder, Colorado, Geological Society of America Special Paper 280, p. 1–44.

Sharry, J., Langan, R. T., Jovanovich, D. B., Jones, G. M., Hill, N. R., and Guidish, T. M., 1986, Enhanced imaging of the COCORP seismic line, Wind River Mountains, *in* Barazangi, M., and Brown, L., Reflection seismology: A global perspective: Washington, D.C., American Geophysical Union, Geodynamics Series, v. 13, p. 223–236.

Skeen, R. C., and Ray, R. R., 1983, Seismic models and interpretation of the Casper arch thrust: Application to Rocky Mountain foreland structure, *in* Lowell, J. D., and Gries, R., eds., Rocky Mountain foreland basins and uplifts: Denver, Colorado, Rocky Mountain Association of Geologists, p. 99–124.

Smithson, S. B., Brewer, J. A., Kaufman, S., Oliver, J. E., and Hurich, C. A., 1979, Structure of the Laramide Wind River uplift, Wyoming, from COCORP deep reflection data and from gravity data: Journal of Geophysical Research, v. 84, p. 5955–5972.

Stearns, D. W., 1978, Fault and forced folding in the Rocky Mountains foreland, *in* Matthews, V., III, ed., Laramide folding associated with basement block faulting in the western United States: Boulder, Colorado, Geological Society of America Memoir 151, p. 1–37.

Stone, D. S., 1984, The Rattlesnake Mountain, Wyoming, debate: A review and critique of models: The Mountain Geologist, v. 20, p. 107–112.

______1991, Analysis of scale exaggeration on seismic profiles: American Association of Petroleum Geologists Bulletin, v. 75, p. 1161–1177.

______1993a, Basement-involved thrust-generated folds as seismically imaged in the subsurface of the central Rocky Mountain foreland, *in* Schmidt, C. J., Chase, R. B., and Erslev, E. A., eds., Laramide basement deformation in the Rocky Mountain foreland of the western United States: Boulder, Colorado, Geological Society of America Special Paper 280, p. 271–318.

_____1993b, Tectonic evolution of the Uinta Mountains: Palinspatic restoration of a structural cross section along longitude 109°15', Utah: Salt Lake City, Miscellaneous Publication 93-8, Utah Geological Survey, 19 p. + 3 plates.

_____2002, Morphology of the Casper Mountain uplift and related, subsidiary structures, central Wyoming: Implications for Laramide kinematics, dynamics, and crustal inheritance: American Association of Petroleum Geologists Bulletin, v. 86, p. 1417–1440.

Varga, R. J., 1993, Rocky Mountain foreland uplifts: Products of a rotating stress field or strain partitioning?: Geology, v. 21, p. 1115–1118.

Wise, D. U., and Obi, C. M., 1992, Laramide basement deformation in an evolving stress field, Bighorn Mountain front, Five Springs area, Wyoming: American Association of Petroleum Geologists Bulletin, v. 76, p. 1586–1600.

MANUSCRIPT SUBMITTED MARCH 21, 2005

REVISED MANUSCRIPT SUBMITTED MAY 29, 2005

MANUSCRIPT ACCEPTED JUNE 3, 2005

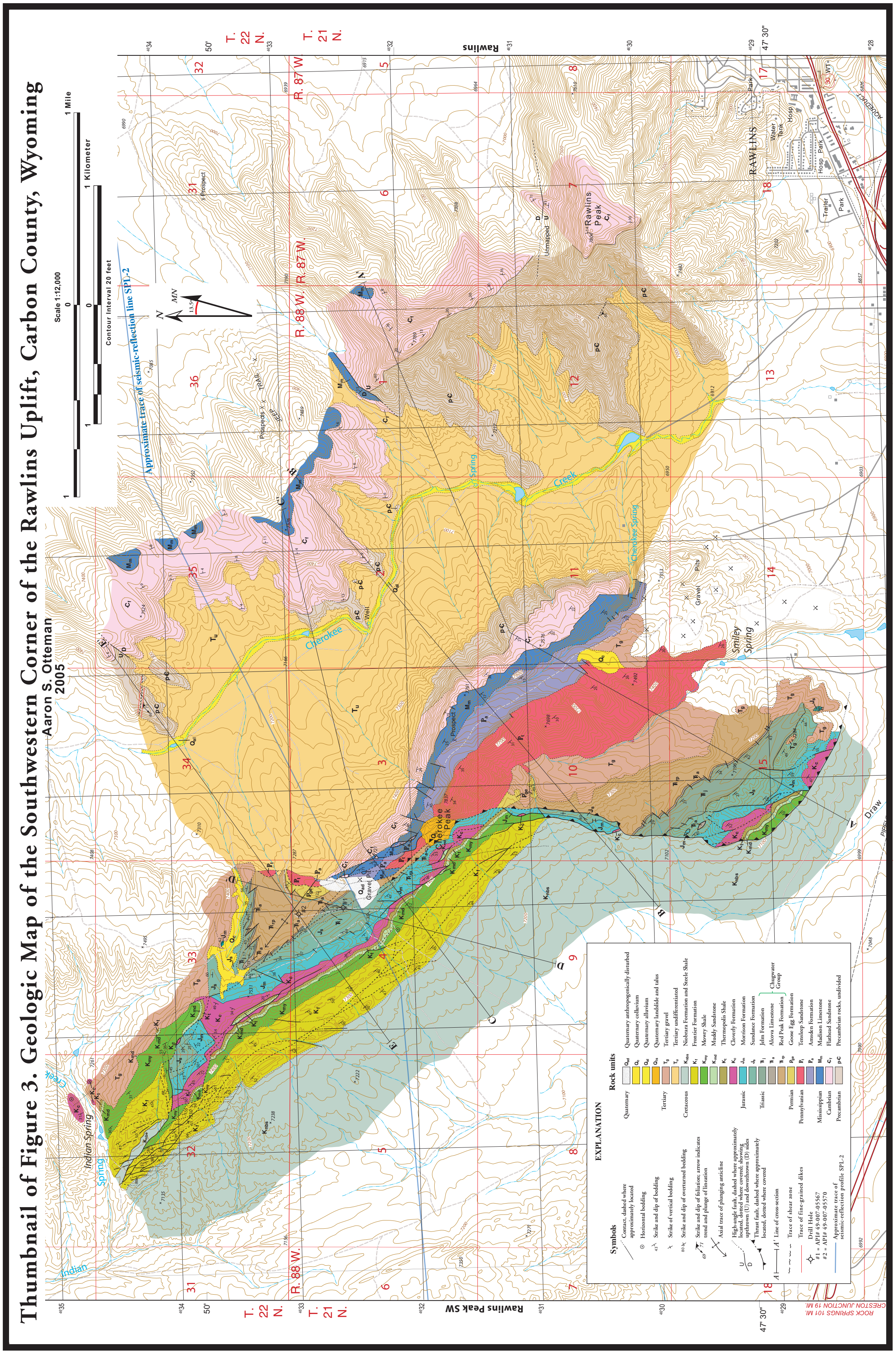
Thumbnail of Figure 3. Geologic Map of the Southwestern Corner of the Rawlins Uplift, Carbon County, Wyoming
Aaron S. Otteman
2005
Scale 1:12,000
Contour Interval 20 feet
1 Mile
1 Kilometer
Approximate trace of seismic-reflection line SPL-2
Rocky Mountain Geology, v.40, no.1
Rawlins
Rawlins Peak SW
RAWLINS
Rawlins Peak
Cherokee Peak
Cherokee Creek
Cherokee Spring
Indian Spring
Smiley Spring
Gravel Pits
T. 22 N.
T. 21 N.
R. 88 W.
R. 87 W.
EXPLANATION
Symbols
Rock units
Quaternary
Tertiary
Cretaceous
Jurassic
Triassic
Permian
Pennsylvanian
Mississippian
Cambrian
Precambrian
Chugwater Group
ROCK SPRINGS 101 MI
CRESTON JUNCTION 19 MI